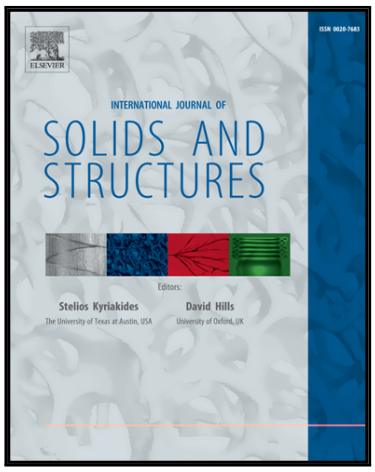

On the Role of Material Architecture in the Mechanical Behavior of Knitted Textiles

Dani Liu , Daniel Christe , Bahareh Shakibajahromi , Chelsea Knittel , Nestor Castaneda , David Breen , Genevieve Dion , Antonios Kontsos

PII: S0020-7683(17)30011-2
DOI: 10.1016/j.ijsolstr.2017.01.011
Reference: SAS 9425

To appear in: *International Journal of Solids and Structures*

Received date: 19 July 2016
Revised date: 6 November 2016
Accepted date: 5 January 2017

Please cite this article as: Dani Liu , Daniel Christe , Bahareh Shakibajahromi , Chelsea Knittel , Nestor Castaneda , David Breen , Genevieve Dion , Antonios Kontsos , On the Role of Material Architecture in the Mechanical Behavior of Knitted Textiles, *International Journal of Solids and Structures* (2017), doi: 10.1016/j.ijsolstr.2017.01.011

On the Role of Material Architecture in the Mechanical Behavior of Knitted Textiles

Dani Liu[1,4], Daniel Christe[1,4], Bahareh Shakibajahromi[2,4], Chelsea Knittel[3,4], Nestor Castaneda[1,4], David Breen[2,4], Genevieve Dion[3,4] and Antonios Kontsos[1,4*]

[1]Theoretical & Applied Mechanics Group, Department of Mechanical Engineering & Mechanics, Drexel University

[2]Department of Computer Science, Drexel University

[3]Shima Seiki Haute Tech Lab, Design Department, Drexel University

[4]Center for Functional Fabrics, Drexel University

Corresponding Author*: e: akontsos@coe.drexel.edu | t: 215-895-2297| a: 3141 Chestnut St, Philadelphia PA 19104

Abstract

Direct numerical simulations based on three dimensional finite element analysis were performed to investigate the mechanical behavior of knitted textiles at the scale where their manufactured material architecture can be simulated and assessed. A numerical investigation of the effects that the material architecture has on deformation localizations, as well as both in- and out-of-plane displacements is presented. To achieve this, a procedure to numerically synthesize and modify knitted textile geometries is investigated which takes into account yarn-to-yarn interactions, while it further allows meshing used in finite element analyses. Appropriate boundary conditions are applied to avoid unnecessary constraints, while a specific type of interaction definition between yarn surfaces is enforced to remove the effect of contact and friction. Furthermore nonlinear analysis is used to capture the geometrically significant yarn position changes resulting from

the flexural motion of the looped knitted textiles. The observed anisotropic effects are explained by examining the load transfer as a function of local material architecture. In addition, both linear and nonlinear material laws are used to study the role of material nonlinearities in the mechanical behavior of this type of material at the length scale of their architecture.

Keywords: knitted textiles, finite element analysis, mechanical behavior, material architecture

Introduction

Functional fabrics are an emerging class of architectured material systems (Ashby, 2013; Barthelat, 2015; Bouaziz et al., 2008) currently used in a variety of applications including defense (Kiekens, 2012; Sun et al., 2009; Sun et al., 2014; Wang, 2012), biomedical (Chapman, 2013; Struszczyk, 2014), and flexible electronics (Lorussi et al., 2013; Park and Jayaraman, 2003; Post and Orth, 2000), among others. Textile manufacturing processes including knitting, weaving, and braiding offer the potential to produce a new generation of material systems with elaborate structural characteristics, which could be extended beyond traditional textile applications. Specifically, the geometrical and topological arrangements achieved for textiles could be used to design metallic, polymeric (Sabantina et al., 2015) etc. lattice-type structures, as already reported in the case of knit-based shape-memory alloy devices (Abel et al., 2013) and ballistic-impact resistant structures (Tran et al., 2014).

Machine knitting refers to the intermeshing of yarns into looped structures using mechanical needle motions (Au, 2011). A wide range of materials are knittable, including cotton, wool, silk (Cook, 1984), shape memory alloys and conductive fibers (Gopalsamy et al., 1999; Marculescu et al., 2003; Park and Jayaraman, 2003). However, despite advances in manufacturing capabili-

ties, a gap still exists in linking the structural characteristics of knitted materials with their overall multiscale mechanical performance. In this context, capturing the three-dimensional geometry of knitted fabrics is integral to their computational modeling. Many investigators have suggested geometrical models, for example, for weft-knitted fabrics (Araujo et al., 2003; Choi and Lo, 2003; Demiroz and Dias, 2000; Hurd and Doyle, 1953; Kurbak and Alpyildiz, 2009; Kurbak and Ekman, 2006; Kurbak and Kayacan, 2008; Kurbak and Soydan, 2009; Leaf and Glaskin, 1955; Miao et al., 2008; Munden, 1959; Peirce, 1947; Semnani et al., 2003; Vassiliadis et al., 2007). The first actual three-dimensional model of the knitted loop (Peirce, 1947) assumed that yarn path along a knitted row lies on a constant cylindrical cross-section, comprising arcs and straight lines. Based on this assumption, Pierce derived geometric relationships involving rows and columns (which are called course and wale in textiles) spacing, as well as the length of yarn forming a loop. In addition, Leaf and Glaskin (Leaf and Glaskin, 1955) demonstrated that the Pierce model gives rise to a non-physical discontinuity in curvature along the loop, and proposed a new model rectifying this shortcoming (Leaf and Glaskin, 1955). Furthermore, Doyle and Munden (Hurd and Doyle, 1953; Munden, 1959) argued that fabric dimensions are primarily governed by the loop or stitch length, and they introduced appropriate structural parameters in relation to the stitch length with values determined through a series of experiments using fabrics in different relaxed states (Munden, 1959; Munden, 1960).

More recent investigations have used cubic splines to represent the knitted loop (Demiroz and Dias, 2000; Kaldor, 2010; Kaldor et al., 2008; Yuksel et al., 2012). Vassiliadis (Vassiliadis et al., 2007) proposed a model for all-knit fabric structures using also course and wale spacing, as well as yarn diameter as initial, independent inputs. Several other investigators attempted to emulate the knitting process itself (Duhovic and Bhattacharyya, 2006; Renkens and Kyosev, 2010). Ren-

kins and Kyosev (Renkens and Kyosev, 2010) used an approach that first formed knitted loops on a flat needle bed, then applied translations and rotations to segments of the structure to transform loops to their positions in three-dimensional coordinates. Moreover, Duhovic and Bhattacharya (Duhovic and Bhattacharyya, 2006) explicitly modeled the knitting process through a dynamic finite element analysis (FEA) simulation to capture the force-determined geometry and residual stresses imposed by manufacturing. This geometry then became the initial state for a virtual tensile test to predict performance of knitted composite preforms. It is also understood that yarns in relaxed states have shapes corresponding to minimum energy configurations (Munden, 1959). Based on this minimum-energy principle, others have attempted to couple mechanics with material architecture through energy-based descriptions of the loop shape (Choi and Lo, 2003; Hearle and Shannanon, 1978; Jong and Postle, 1977; Munden, 1959).

Furthermore, due to the hierarchical structure and large area-to-thickness ratio of fabric materials, computational homogenization methods and multi-scale analysis have been used to investigate mechanical properties and responses at the macroscopic level. Most studies were conducted for plain woven fabrics, which represent a common reinforcement of textile composites. Based on a nested homogenization developed for heterogeneous thin sheets (Coenen et al., 2010; Geers et al., 2007), a generalized stress-strain response at the macro shell level was obtained from an appropriate averaging of the Representative Volume Element (RVE) response at the microscale level for woven (Fillep et al., 2013; Green et al., 2014) and rope-type textiles (Fillep et al., 2015). The macroscopic features obtained from classical homogenization methods, built based on averaging theorems and RVE models, were further applied in the simulation of a structural cylinder for screen printing applications (Carvelli et al., 2008). Effective non-classical mechanical properties were deduced based on a couple-stress model for dry woven textiles, which indi-

cated size-influenced properties (Rahali et al., 2016). However, such investigations addressed only partially the issue of RVE existence, the definition of which is not well understood for textile materials, and especially for knitted fabrics. Additionally, models based on the assumption of a constitutive law at the macroscale, derived analytically (Nadler et al., 2006) or based on experiment results (Yeoman et al., 2010) have been suggested to simulate the macroscale fabric behavior. This approach, however, becomes practically infeasible and inaccurate for textiles with intricate microstructures or under complex loads.

Direct studies of the mechanical performance of textile materials have also been reported. Specifically, an analytical treatment of the buckling behavior for knitted fabrics was performed using constitutive modeling and stability theory (Zhang et al., 2005; Zhang et al., 2007). With the aid of unit cell definition and periodic boundary conditions, FEA under different loading cases demonstrated mechanical responses similar to experiment results (Gasser et al., 2000; Lin et al., 2009; Vassiliadis et al., 2007). Furthermore, the bagging behavior (Karimian et al., 2014) and manufacturing process (Duhovic and Bhattacharyya, 2006) were investigated for textiles using FEA. For woven fabrics made of high strength fibers, ballistic analysis is of great interest, which has been investigated using 3D FEA with boundary conditions derived based on the experiment conditions (Barauskas and Abraitienė, 2007; Duan et al., 2005). However, the periodicity assumption and unavoidable size effects on the direct simulation not only cause an obvious deviation from the real behavior but also require a significant computational cost making such approaches computationally challenging.

It is widely accepted that the role of textile architecture in determining the macroscopic behavior is still not yet adequately described by either the traditional homogenization approach or existing direct numerical simulations. In this context, the purpose of the research reported in this article is

to provide a novel view in addressing the challenge of linking structural and material properties with the mechanical behavior of knitted textiles. To this aim, monolayer textile architectures (Carvelli et al., 2008; Fillep et al., 2013; Maruccio et al., 2014) are simulated and key attributes of the overall mechanical behavior at the length scale of the architecture of knitted textiles are investigated, including the 3D nature of deformation and mechanical anisotropy, as well as the evaluation of the effect caused by intrinsic parameters of the models including the contact definition and curvature of the knitted loops.

Geometrical Modeling of Knitted Loops

Yarns comprised of bundles of filaments or staple fibers represent the basic structural element of fabrics. In knitted fabrics such yarns take the form of loops, created by drawing the yarn through the loop from the previous row. A stitch that is drawn through the previous loop from back to front is called a 'knit' stitch, whereas a 'purl' stitch is created when the stitch is drawn through the previous loop from front to back. In knitting nomenclature, wales denote "columns" of stitches which are produced by a single knitting needle over multiple knitting cycles (Au, 2011; Kothari, 2011; Spencer, 2001). Courses refer to "rows" of stitches, produced by a set of knitting needles in a single knitting cycle (Au, 2011; Kothari, 2011; Spencer, 2001).

Based on this description of the so-called "stitch geometry" of knitted textile architectures and by following an approach previously reported (Peirce, 1947; Vassiliadis et al., 2007) three fundamental input parameters were used to generate models of the plain knitted loop. These are the wale spacing (W), course spacing (C) and yarn diameter (D), illustrated in Figure 1 by an optical microscopy image of a knitted material manufactured by the authors. The simplest possible knitting pattern (Spencer, 2001) known as the "jersey knit", comprises entirely "knit" stitches as

shown in Figure 2. For this knitted textile specimen manufactured by using a Shima Seiki SSG122SV knitting machine, an optical microscopy image of its local material architecture and a higher magnification digital microscopy image of the type of contacts formed due to knitting are provided to illustrate the type of geometrical details that need to be captured while numerically synthesizing textile architectures.

Figure 1: An illustration based on an optical microscopy image of the geometrical parameters that are used in this article to define the architecture of knitted textiles: course spacing (C), wale spacing (W), yarn diameter (D).

The mechanical properties and performance of the yarn are dictated by factors including material composition, fiber lengths (staple vs. filament) and quantity of the constituent filaments or plies. Intricate phenomena of untwisting, varying stiffness and additional dissipation arise for knitted materials made of multi-filament yarns (Schwartz, 2008). In this article, emphasis is placed on jersey knitted fabrics comprised of monofilament yarns (Figure 2), to mitigate yarn twist-related effects and reduce the number of parameters that are explored by the computational approach in terms of linking the effect of architecture on the mechanical behavior of such material systems.

The knitting process imparts residual stresses to the manufactured textiles (Choi and Lo, 2003; Duhovic and Bhattacharyya, 2006). Hence, immediately after knitting is performed, inter-yarn

forces are responsible for providing the shape of the knitted loops (Choi and Lo, 2003). Given sufficient time, the fabric relaxes to a lower energy configuration, in which torsional and bending properties of the yarn material itself become dominant and ultimately define the final loop shape (Choi and Lo, 2003). These factors are not included in the computational approach presented in this investigation since the focus is on generating geometrical models of constant yarn cross section with the intent to focus on issues that relate to the 3D geometry, yarn-to-yarn contact properties and material used, and not into obtaining specific values related to their mechanical behavior.

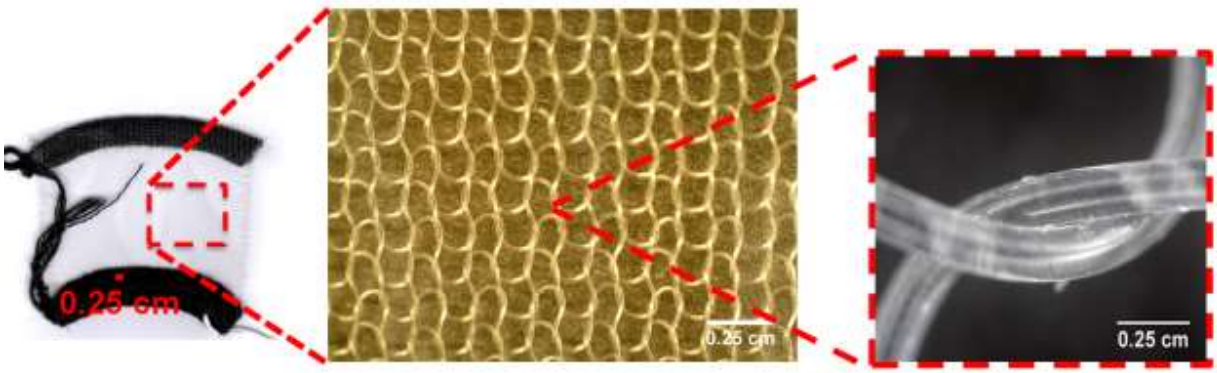

Figure 2: (left) A jersey-knitted fabric specimen manufactured by the authors on a Shima Seiki SSG122SV knitting machine; (center) an optical microscopy image of its architecture and (right) a higher magnification digital microscope image of a yarn-yarn contact.

To computationally design stitch geometries for knitted textiles, the architecture of the jersey-knit shown in Figure 3(a) was examined both in terms of its loops as well as its symmetries. This geometrical model comprises four different yarns designated by the yellow, blue, green and red colors. For reference purposes in the remainder of this text, the knit model in Figure 3(a) is called a "3x3", as three rows in the course and 3 columns in the wale direction can be seen. Analyzing further the architecture in Figure 3(a) it is proposed herein that the structural assembly on

the bottom of Figure 3(a) is the repeating building block of the entire structure. Hence, this assembly in the form of a "half-loop" that connects two different yarns is called a unit cell in this article, in reference to the term that has been used to denote similar repeating units in the field of micromechanics. By changing this unit cell, different material architectures for the same type of stitch pattern (i.e. jersey knit in this case) can be produced, demonstrating the capability to produce a plethora of novel 3D architectures. Specifically, Figure 3(b) has a unit cell with different curvature of the red yarn, while Figure 3(c) shows a unit cell in which the interyarn contact has been modified with respect to the unit cell in Figure 3(a). It should be noted that at this stage of modeling the manufacturability of such yarn operations was not of direct concern.

A closer look at Figure 3(a) shows that the spatial arrangement of the knit architecture includes six connectivity points, denoted by A~F, which connect the central unit cell to four other adjacent ones forming the cross-type pattern denoted by the dotted lines. This observation is important as it could assist the numerical generation of such material architectures of arbitrary dimensions. Overall, a hierarchical view of the type of material architecture found in 3D knitted textiles is presented herein with the goal to understand how changes in geometrical and topological parameters, as shown later in this article, relate to changes in the mechanical behavior of such materials.

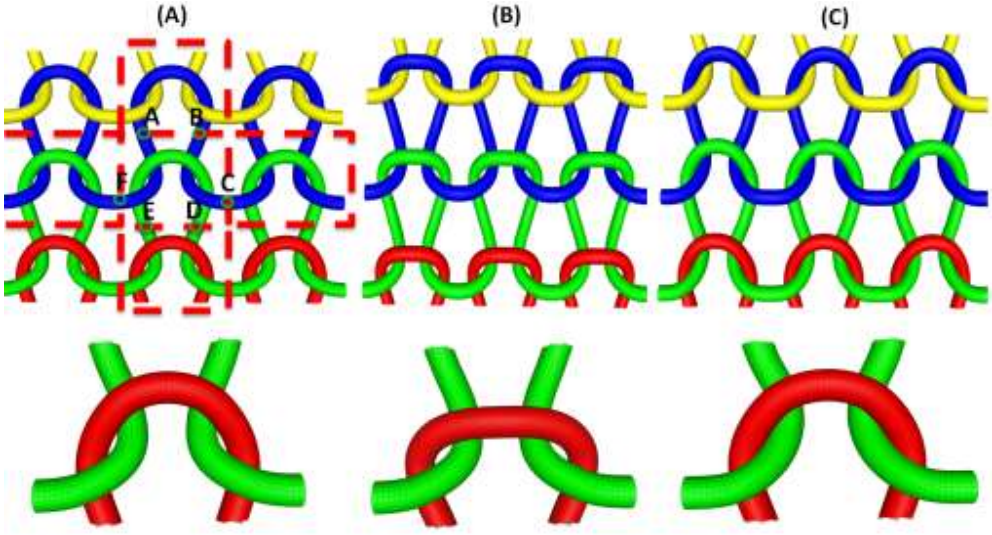

Figure 3: 3D digital representations (top) and accompanying unit cells (bottom) of the jersey-knitted fabrics investigated in this article. (a) Original jersey knit structure, (b) jersey knit with different curvature, and (c) jersey knit with larger inter-yarn contact area.

To create the digital representations of knitted textiles shown in Figure 3 and 4, custom input scripts were written for a publicly available software package (TexGen) (Lin et al., 2012) to create yarn centerlines which were represented with piecewise cubic Bezier curves (Farin, 2001) using a Catmull-Rom construction (Catmull and Rom, 1974). In the most general form a polynomial spline consists of segments $\mathbf{S}_i(u)$: $[u_i, u_{i+1}] \rightarrow \mathbb{R}$, so that if a set of points

$$u_0 < u_1 < \cdots < u_{n-2} < u_{n-1} \tag{1}$$

is defined then the spline segments can be defined as

$$\mathbf{S}(u) = \begin{cases} \boldsymbol{S}_0(u), & u_0 \le u < u_1 \\ \boldsymbol{S}_1(u), & u_1 \le u < u_2 \\ & \cdots \\ \boldsymbol{S}_{n-2}(u), & u_{n-2} \le u < u_{n-1} \end{cases} \tag{2}$$

Specifically, piecewise cubic Bezier curves are defined by four points (say $\mathbf{P_1}$, $\mathbf{P_2}$, $\mathbf{P_3}$, and $\mathbf{P_4}$) in 3D space. In this case, the parametric equation for a single cubic Bezier curve **B** can be written as:

$$\boldsymbol{B}(u) = \boldsymbol{P_1}(1-u)^3 + 3\boldsymbol{P_2}u(1-u)^{\mathbf{2}} + 3\boldsymbol{P_3}u^2\,(1-u) + \boldsymbol{P_4}u^3 \tag{3}$$

To preserve C^0 continuity, $\mathbf{P_{1i}}$ and $\mathbf{P_{4i}}$ for a spline segment $\mathbf{S}_i$ are defined as:

$$\mathbf{P_{1i}} = \boldsymbol{S_i}(u_i) \quad 0 \le i \le k-2 \tag{4}$$

$$\mathbf{P_{4i}} = \boldsymbol{S_i}(u_i) \quad 0 \le i \le k-2 \tag{5}$$

In this work, fifteen control points which define the end-points of the individual Bezier curves, (Figure 4) were used to provide greater control over yarn-to-yarn intersection points – the original version of the knitted loop source code can be found in (Sherburn, 2007). A constant circular cross-section (Lin et al., 2012) of diameter (D) was then swept along the centerline to form a yarn. This 3D geometry can be used to create a volume mesh (Lin et al., 2012; Sherburn, 2007) for finite element simulations. Given n-equally spaced points along the boundary of the cross-section, a rectangular grid is overlaid on the yarn cross-section. The elements are split into c columns and r rows, and the nodes defining each element are split into c+1 columns and r+1 rows. The relationship between n, c, and r is given as (Sherburn, 2007)

$$n = 2(c+r) - 4. \tag{6}$$

This method requires that n and r are even numbers, to have a symmetric mesh about the x- and y- axes. Further details on this meshing procedure can be found in (Sherburn, 2007). In Table 1, the actual geometrical parameters used for the models in this article are listed and are based on measurements made on the optical microscopy images of Figure 2. An average of those meas-

urements was then used to obtain the wale and course spacing values, while the diameter value agreed with the diameter of the fishing line yarn used to manufacture actual specimens with an automatic knitting machine (Shima Seiki SSG 122 SV).

Table 1: Geometrical parameters for the three models used in this study (units of mm)

Wale Spacing (W)	12
Course Spacing (C)	16
Diameter (D)	2

This procedure of 3D loop generation often produces geometries with significant yarn-to-yarn interpenetration (Kyosev et al., 2005). Resolving interpenetration is a non-trivial challenge, and several approaches have been proposed in textile modeling, based on pure geometric optimization (Brown et al., 2013; Zeng et al., 2014) or variational energy-based methods (Hearle and Shannanon, 1978). In this investigation, the control points were manually adjusted near the contact areas, while monitoring the interpenetration depth to achieve contact conditions without large overclosure or interpenetration between yarn surfaces, an example is shown in Figure 5. Finally, a local coordinate system was automatically implemented along each yarn to specify the material orientation. Hence, the local material axis ‘1’ lies along the tangent of the underlying path line, while axes ‘2’ and ‘3’ are in the transverse plane and arranged according to the right hand rule.

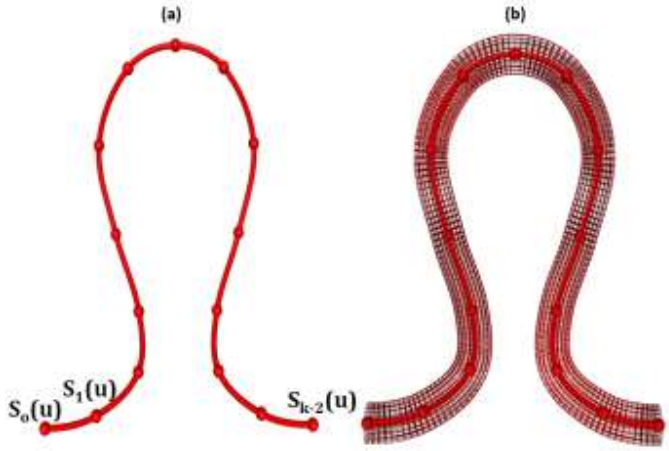

Figure 4: Definition of yarn centerlines using a set of 15 control points and an interpolating spline. A constant radius circular cross-section is assumed around such centerlines to form a 3D yarn model which can be also meshed for subsequent finite element simulations.

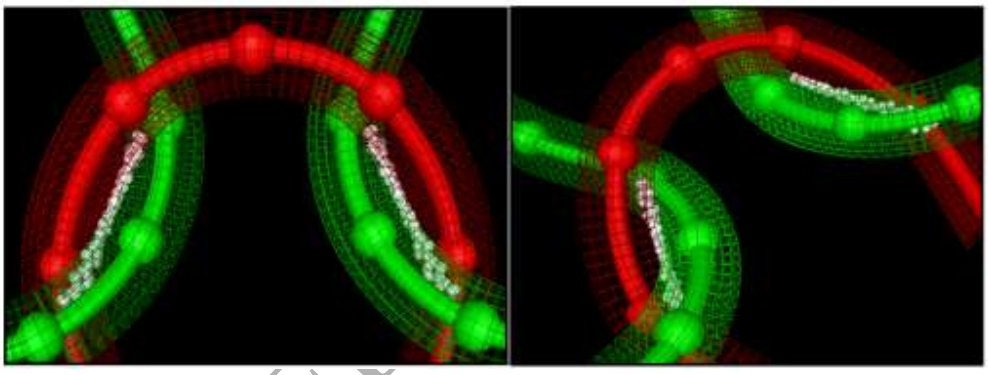

Figure 5: Interpenetration between yarns is quantified by the white balls. The adjustment described in this article reduced such overlapping areas.

Simulation Methodology

Geometrical models defined based on the approach described in the previous section were imported to a commercially available FEA code (ABAQUS 6.13/Standard) and the following procedure was used to set up boundary value problems and obtain results related to the mechanical behavior of knitted textiles.

Boundary conditions and mesh

The boundary conditions for the direct numerical simulations in this article are shown in Figure 6(a). Specifically, all translational degrees of freedom of the left side nodes were fixed for displacement-controlled tensile loading in the course (horizontal) direction, while all nodes on the top and bottom of the 3D model in Figure 6(a) were free. Similarly, for wale tension the bottom edge nodes were fixed and the top nodes were used to apply displacement along the wale (vertical) direction. The free boundary conditions used allowed natural contraction and rotation in the transverse direction perpendicular to the tensile load applied either in the course or wale direction, which creates a much more flexible and realistic constraint condition that is independent of the influence of adjacent material as compared to the case of periodic boundary conditions that are frequently applied (Gasser et al., 2000; Lin et al., 2009; Vassiliadis et al., 2007). Linear hexahedron elements with reduced integration method were used and a mesh sensitivity analysis was performed in the case of course tension loading, as shown in Figure 6(b). The applied strain in the course direction was measured at the global level, and therefore it was defined herein as the ratio between the applied displacement a and the total course length. By summing up the reaction forces in the load direction over all fixed nodes, the total reaction force at an arbitrarily selected 5% imposed course strain was obtained to evaluate the mesh influence using three different mesh resolutions of R10, R20 and R24 as shown in Figure 6(b), which demonstrates a converging trend. Detailed information about the total number of elements and degrees of freedom can be found in Table 2. To ensure computational efficiency and based on this study, the R20 mesh resolution was adopted for all simulations in this investigation.

Table 2: Total number of elements and degrees of freedom for different mesh resolution

Mesh Resolution	Number of Elements	Degrees of Freedom
R10	7,650	32,562
R20	48,960	189,513
R24	87,696	325,260

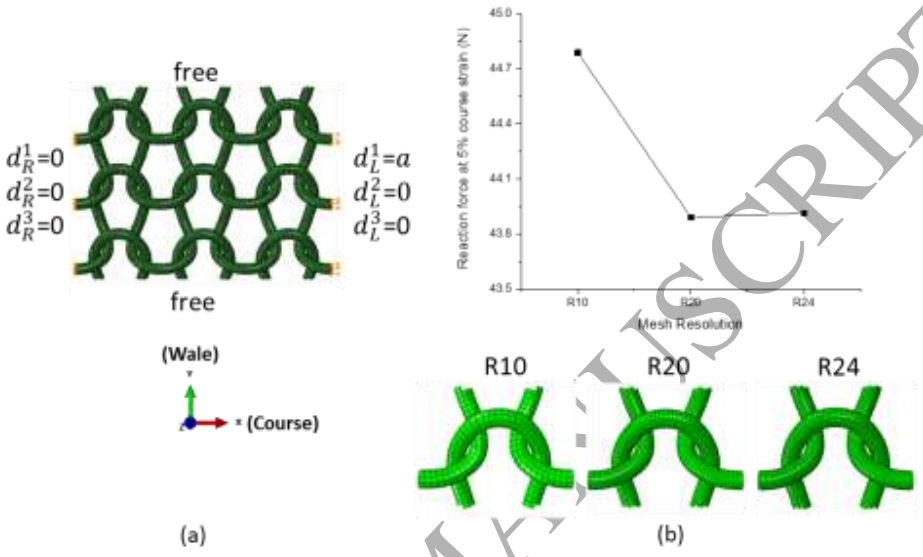

Figure 6: (a) Boundary conditions for course tension (b) Mesh sensitivity analysis for resolution 10, 20 and 24 under course tension.

Yarn-to-yarn interactions

The interactions between yarns, including sliding, compression of one yarn to another and rotation represent intricate features of the deformation and motion of a knitted material. Relative normal and tangential movement of the yarn interfaces result from contact and friction, which also contribute to their observed nonlinear behavior. To investigate the effect of such factors on the material behavior, an account of the complex contact-friction behavior was needed. To this aim, a tie constraint was built to simplify this aspect of the problem, by which each of the nodes of the so-called slave surface was forced to have the same displacement as the corresponding nodes of the master surface (ABAQUS, 2013). 'Surface-to-surface' discretization was also used to minimize numerical noise by enforcing constraints in an average sense over a finite region in-

stead of performing such minimization at discrete points on the master surface. In addition, the displacement was interpolated as:

$$u_0 + \sum_{i=1}^{n} A_i u_i = 0 \quad (7)$$

where u_0 and u_i are the displacements of the slave and master nodes, A_i is the tie coefficient and n is the total number of master nodes, which are assigned and adjusted for each increment by the FEA code. As the current geometry modeling method fails to provide yarn interfaces that are in perfect contact at least in the initial configuration before relaxation, a position tolerance (d_{tol}) of 10% of the slave facet diagonal length was applied to determine which slave nodes will be tied to the master surface. Any node on the slave surface whose distance to the master surface was within the d_{tol} was moved to the master surface in this initialization process before the first increment, and the resulting configuration remained unchanged during the whole loading process.

Geometric nonlinearity

The flexural motion of the internal structure of knitted materials adds nonlinearity into the overall mechanical behavior, even for models without contact and friction definition or under a finite global deformation. The geometric nonlinearity option in the FEA code was therefore used which allows the element stiffness matrix to be updated at every increment using the Newton-Raphson algorithm that solves the resulting nonlinear problem. To achieve this, the discretized form of the iteration equation can be expressed as follows:

$$K_i^{NP} c_{i+1}^{P} = -F^N(u_i^M) \tag{8}$$

where

$$K_i^{NP} = \frac{\partial F^N}{\partial u^P}(u_i^M) \tag{9}$$

is defined as the Jacobian matrix. At the i^{th} iteration, c_{i+1}^{p} is the deviation of the approximation u_i^p from the exact solution and F^N is the force component conjugate to the N^{th} variable. A complete Jacobian matrix consists of the small-displacement stiffness matrix accounting for a material constitution relationship based on generalized strain measurements, initial stress matrix resulting from pre-stress hardening and load stiffness matrix caused by external load.

When the geometric nonlinearity is activated in the simulation, local DOFs are allowed to rotate in each element, which results in additional displacements that affect the Jacobian matrix assembly process. Hence, the Jacobian matrix is updated in this case at each loading increment to consider the influence of various nonlinear effects, including a nonlinear material law definition, large deformation caused by rigid body motion or boundary nonlinearity caused from the contact definition. By using the tie constraint described above and a linear isotropic material law, flexural-motion-based changes in the Jacobian matrix become the only source of the nonlinearity, the effect of which can therefore be investigated.

Material Properties

Most knitted textiles are composed of multifilament yarns, which lead to a crushing behavior in the transverse plane with respect to the yarn's longitudinal direction (Lin et al., 2008). In addition, material stiffness changes as a function of the evolving loading state due to the loose internal structures of the yarn. However, a nonlinear crushing response can be avoided in the case that

a monofilament yarn is used, which is the case of the investigation in this article. In this context, a linear isotropic constitutive law with elastic properties of polypropylene was used in most of the simulations in this article, and the corresponding properties are listed in Table 3. To test the limitations of this assumption, both an isotropic steel material and an isotropic, hyperelastic Mooney-Rivlin model were used to describe rubber behavior and quantify the effect of this parameter on the overall mechanical behavior. The elastic strain energy density of the Mooney-Rivlin model was used, which is defined as:

$$U = C_{10}(\bar{I}_1 - 3) + C_{01}(\bar{I}_2 - 3) + \frac{1}{D_1}(J-1)^2 \tag{10}$$

where C_{10}, C_{01} and D_1 are material constants, J is the elastic volume ratio, $\bar{I}_1$, $\bar{I}_2$ are first and second invariants of the deviatoric strain defined as:

$$\bar{B} = \bar{F} \cdot \bar{F}^T \tag{11}$$

where,

$$\bar{F} = J^{-\frac{1}{3}}F \tag{12}$$

and F is the deformation gradient. Incompressibility was enforced by setting D_1 to zero.

Table 3: Material properties and constants

Linear (polypropylene)	$E = 1.34\ GPa, \nu = 0.42$
Linear (Steel)	$E = 200\ GPa, \nu = 0.29$
Hyperelastic (Rubber)	$C_{10} = 176050, C_{01} = 4332, D_1 = 0, \nu = 0.42$

Results and discussion

3D Stress State, Size Effect and Anisotropy

The stress distribution of the knitted textile subjected to a 5% course tension strain appears in Figure 7 to be complex as a result of the architecture of the material. Specifically, at the front side view shown in Figure 7(a), both compressive and tensile states occur simultaneously due to the 3D yarn position changes that include both motion (translation/rotation) and deformation/stretching, justifying the complexity caused by the material architecture and the connectivity in this type of materials. In addition, a non-uniform out-of-plane stress is developed around the contact areas, shown in Figure 7(b). This complicated 3D stress state suggests that given the boundary and loading conditions both the deformation and ultimately the failure (not investigated in this article) of this type of material could be strongly dependent on the material architecture as Poisson effects alone are not capable of explaining the types of stresses obtained.

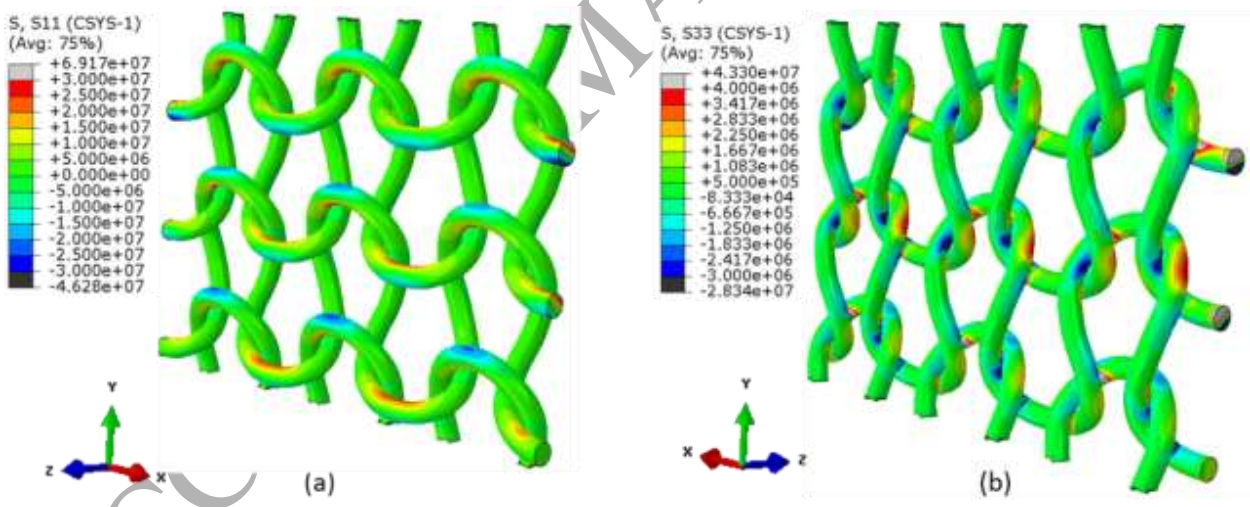

Figure 7: 3D stress state caused by 5% course tensile strain: (a) compression and tension stresses developed near the contact points, and (b) out-of-plane stresses.

Figure 8(a) demonstrates that the out-of-plane stresses shown in Figure 7(b) also cause an overall out-of-plane shape under course tension, which is similar to buckling that appears in shell or plane structures. This type of out-of-plane deformation, as mentioned earlier, appears to be the combined result of Poisson and material architecture effects. To better investigate this structural behavior, size analysis was performed and the results are shown in Figure 8. In Figure 8(a), the maximum out-of-plane displacement U3 is shown to occur near the geometric center of this structure. For different material domain sizes including a 3×3, 6×6 and 8×8 models, this out-of-plane displacement was computed to be equal to $1.942 \times 10^{-4}m$, $3.717 \times 10^{-4}m$ and $4.75 \times 10^{-4}m$, respectively for an imposed 5% course strain. In fact, at a specified strain value, not only the maximum U3 increases with the domain size, but the increasing rate of U3 is also greater for a larger material domain, which is shown for a range of imposed course strains shown in Figure 8(b). The size effect is actually partly coming from the reduced influence of the boundary, but is mainly caused by the shell-shaped global structure and the internal entanglement of the yarn. Moreover, the increase of the out-of-plane displacement as a function of imposed strain actually decreases with the enlargement of the material domain, showing a tendency of convergence in terms of overall model size.

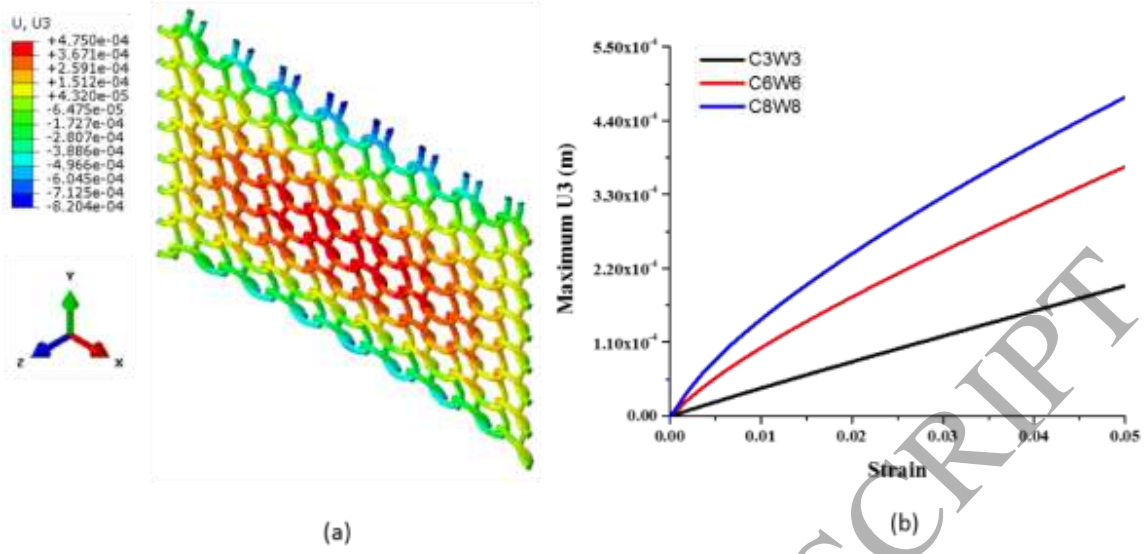

Figure 8: Comparison between different domain sizes for (a) out-of-plane displacement contour (b) maximum out-of-plane displacement versus strain curve.

Furthermore, Figure 9 clearly shows that the knitted model responds differently to tensile loads applied in the course and wale directions. Specifically, the out-of-plane displacement contours for the course and wale directions are displayed in Figure 9(a) and (b), respectively, both of which as a response to a 5% imposed strain in each direction. Despite the relatively greater maximum reaction force value computed in wale tension compared with the course tension case, 'buckling' due to a localized deformation in the center area does not occur when the knitted material is undergoing a wale direction stretch. The transverse contraction for wale tension is also greater than that for course tension, which clearly indicates the influence of local material architecture in the overall mechanical behavior. In addition, the reaction force versus imposed strain curves in Figure 9(c) reveal a much stiffer behavior in the wale direction.

To explain this deformation anisotropy, an illustration of the possible load transfer path in these simulations is shown schematically in Figure 9(d). Specifically, load in general could be transferred mainly through the wavy path defined by the loops and connection points. This path in the

course direction is different compared to the corresponding one in the wale direction. Actually, the fact that the path in the wale direction appears to be less wavy is related to the way the loop material is stretched versus deformed as a 3D curved structure. In fact, the apparent stiffness to unfold an originally curved/looped member can be easily shown to be smaller compared to the axial stiffness of a corresponding straight member, which in part explains the effect of overall material architecture in the resulting mechanical behavior computed by the knit models in this investigation. Thus to connect this finding with manufacturing of knitted textiles, a stiffer behavior with respect to any axial loading can possibly be achieved if the yarn waviness decreases.

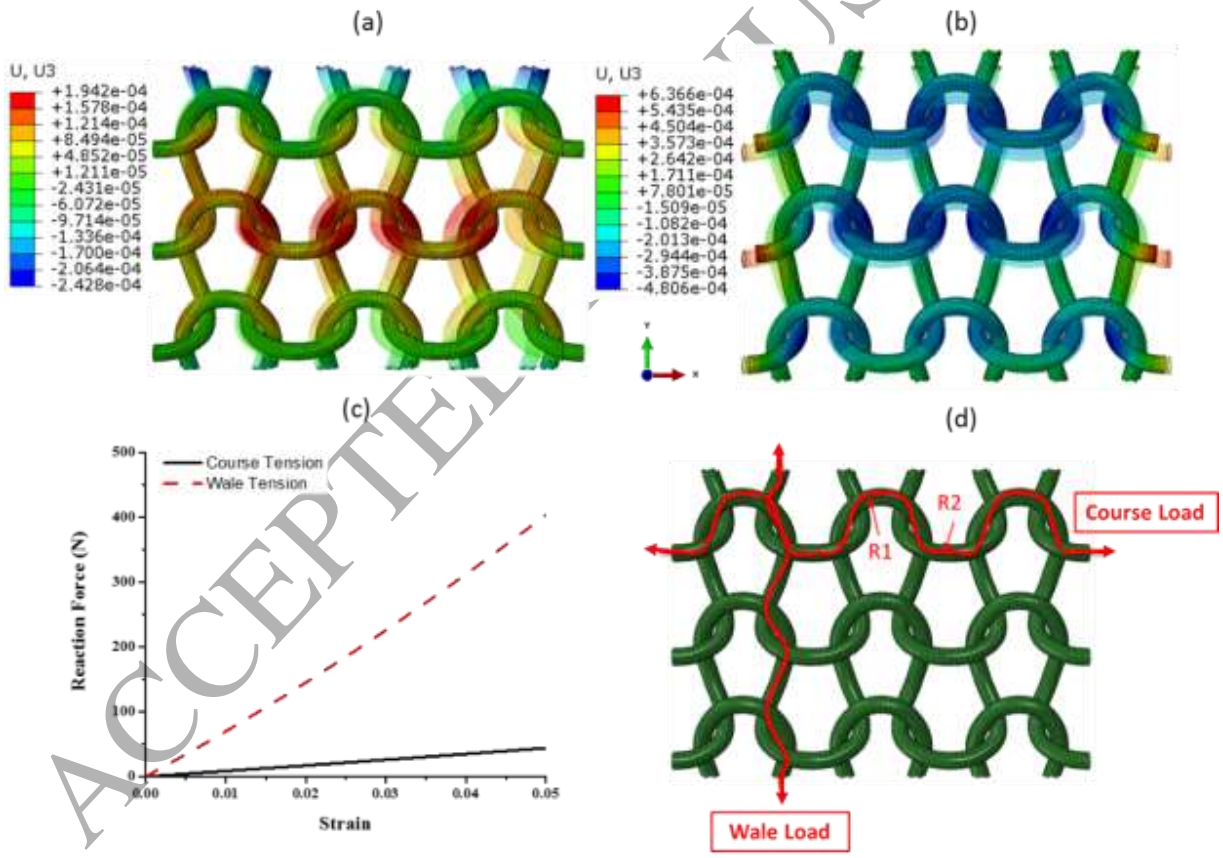

Figure 9: Out-of-plane displacement for (a) 5% course tension (b) 5% wale tension, comparison of the (c) reaction force versus strain curve and (d) load transfer path.

To demonstrate this effect a less wavy path was designed in the course direction by reducing the curvature of the loops as shown in the textile structure named as "B" in Figure 10(a) compared to the original structure names as "A" for which results were previously reported. Based also on the results shown in Figure 9, it is demonstrated in Figure 10(a) that the maximum out-of-plane displacement changes from $1.942 \times 10^{-4}m$ to $2.384 \times 10^{-4}m$ when the curvature is smaller, while the out-of-plane displacement contour remains consistent between the two models demonstrating the shell-shaped behavior. Furthermore, the reaction force versus imposed strain curves in Figure 10(b) support the load transfer illustration and appended hypothesis in Figure 9(d) related to the effect that the reduced curvature along the course direction should have on the structure. Specifically, the reduced curvature model "B" resulted in a stiffer structure as predicted.

In addition to the curvature of the loop geometry, yarn-to-yarn interfaces also play an important role in the mechanical behavior of knitted textiles. Intuitively, the larger the contact area the more effective such load transfers become, resulting also possibly to reduced stress/strain concentrations. The direct assessment of this hypothesis proved challenging as difficulties were encountered in controlling the contact area using the available numerical tools. To mitigate these challenges, a new model with an overall modified (but not quantitatively assessed) contact area was built and the new textile structure was named model "C". A comparison of the original model "A" and the new model "C" showed that the maximum out-of-plane displacement of structure C that has the modified contact area, changes as listed in Table 4. In addition, the reaction force and strain curves in Figure 11 demonstrate differences also in the overall behavior. Interestingly and by taking into account the results reported earlier in this article, a trend appears indicating that an overall reduced out-of-plane deformation is always accompanied by a decrease

of the apparent stiffness quantified as the slope in the reaction force versus imposed strain plots in this article.

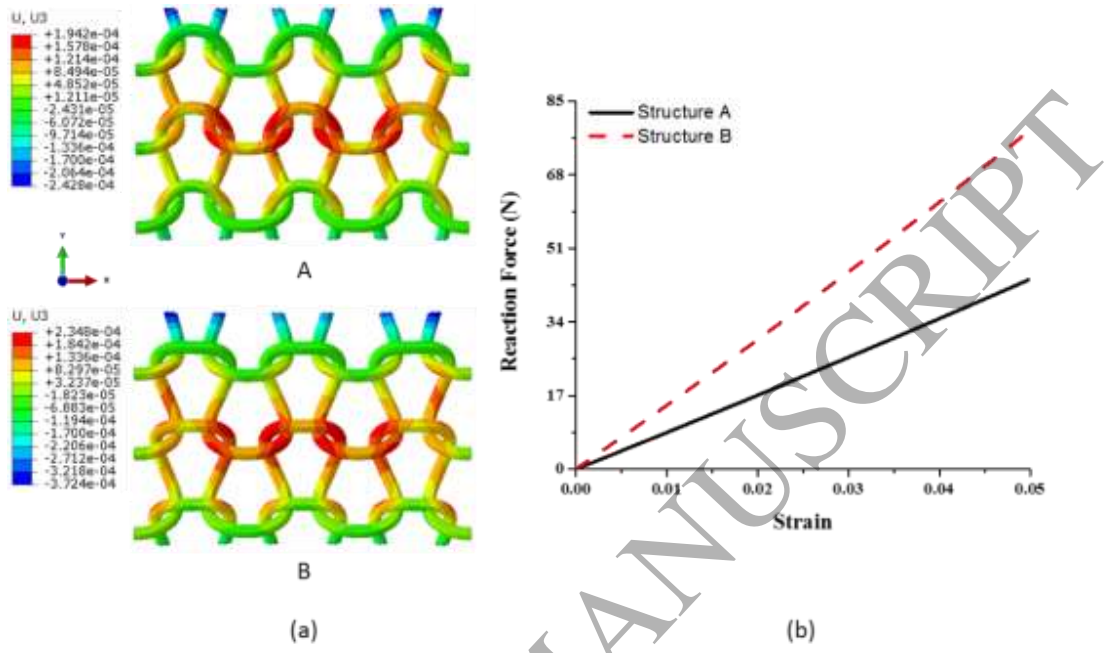

Figure 10: Comparison between structure A and B of (a) Displacement contour in z direction under 5% course tension for Polypropylene and (b) reaction force versus strain curve.

Generally, material behavior is not only governed by architecture but also depends on the properties of the constituents. Therefore, keeping the microstructure unchanged, a simulation with different yarn material properties was performed. As shown in Table 4, it is interesting to note that the maximum U3 for steel, keeping the material architecture the same, was calculated to be equal to $1.98 \times 10^{-4} m$, which is only 2% different compared to the polypropylene case, although the Young's modulus ratio between the two materials is equal to about 150. Based on these findings, it is argued that the material architecture in 3D knitted textiles plays a dominant role in their mechanical behavior at least at the length scale investigated herein.

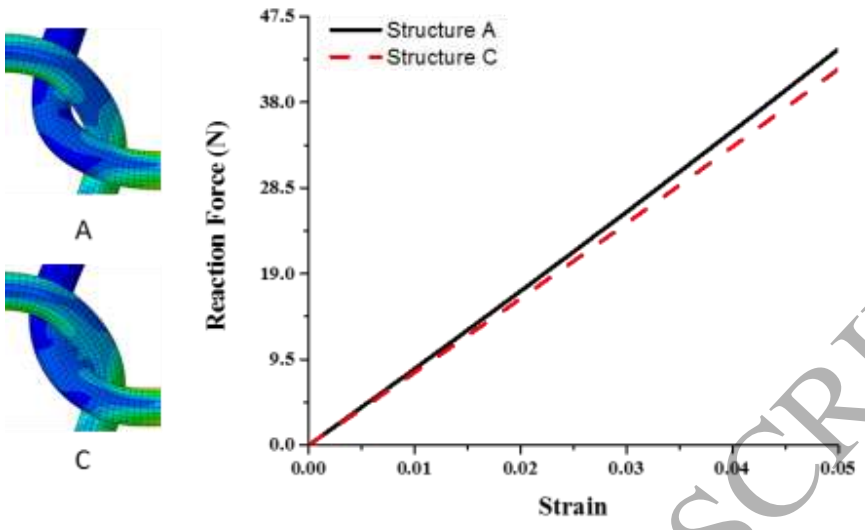

Figure 11: Comparison of the reaction force versus strain for models with different contact area and the same yarn material (polypropylene).

Table 4: Maximum out-of-plane displacement: unit (mm)

Structure A, Polypropylene, 5% course strain	1.942×10^{-4}
Structure B, Polypropylene, 5% course strain	2.384×10^{-4}
Structure C, Polypropylene, 5% course strain	1.771×10^{-4}
Structure A, Steel, 5% course strain	1.98×10^{-4}
Structure A, Polypropylene, 25% course strain	1.002×10^{-4}
Structure A, Rubber, 25% course strain	1.001×10^{-4}

As mentioned earlier, geometric nonlinearity caused by flexural displacement contributes to the nonlinear behavior of knitted textiles. To this aim, relatively small strain levels (5%) were imposed in the simulations used to produce the results previously reported to reduce the effect of such nonlinearity effects. Hence, to obtain a better understanding of structural versus material effects, material nonlinearities were also added into the model. Specifically, the response of the knitted textile with a hyperplastic yarn subjected to 25% course tension was investigated in Fig-

ure 12(a). Slight differences of the maximum out-of-plane displacement were found between the polypropylene ($1.002 \times 10^{-4} m$) and rubber case ($1.001 \times 10^{-4} m$) when both were stretched to 25% in the course direction, as reported in Table 4. It is worth noticing that although some of the global effects such as the overall out-of-plane deformation were not found to change by considering the material nonlinearity, local information was found to be different compared to the globally applied strain. Specifically, by plotting the logarithmic strain (defined by ABAQUS as the numerically time integrated strain increment applicable in the case of nonlinear analysis), denoted as LE11, in Figure 12(a) it became clear that at a local level the structure is capable of accommodating a portion of the imposed strain as the maximum logarithmic strain in the course direction LE11 was found to be equal to 14.86% compared to the imposed 25% strain in the course direction. However, even for this reduced local strain the material nonlinearity effect still exists, demonstrated by the fact that the stress-strain curve (plotted using the definition given in Equation (10)) in Figure 12(b) for rubber is in the nonlinear regime for this amount of strain, while the corresponding polypropylene material follows the linear isotropic behavior denoted by the dashed blue line. Consequently, the effect of material nonlinearity was found to not significantly affect this type of local and global mechanical behavior attributes.

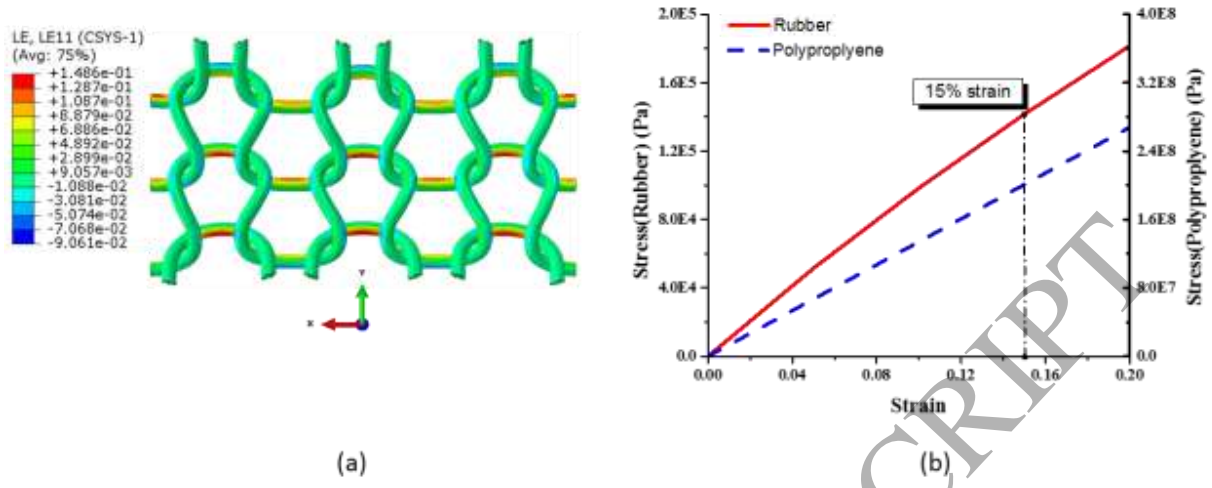

Figure 12: (a) strain contour LE11 under 25% course tension for rubber with Mooney Rivlin model and (b) comparison of stress strain curve under uniaxial tension with Polypropylene

Conclusion

In this investigation, direct numerical simulations using finite element analysis for knitted textiles are presented to investigate the role of material architecture on the mechanical behavior of knitted textiles. To perform such simulations, the architecture of such materials is modeled explicitly using a combined mathematical representation and digital visualization that allows both the identification of important information related to the fundamental building block of such geometries, as well as the definition of neighboring yarn-to-yarn interactions. Meshing of such digital geometries allowed their use in finite elements simulations which involved 3D models with non-periodic boundary conditions to account for the shell-type behavior of knitted textiles. Geometry-dominated three dimensional states of deformation were computed which further showed a strong anisotropy between the course and wale directions of knitted textiles, as well as a pro-

nounced out-of-plane displacement due to Poisson and local interaction effects. Such characteristics were further investigated as a function of the geometry and yarn-to-yarn interactions of such materials, revealing mechanical behavior effects that are structure-dominated. These effects were further explained by considering the load transfer capability of knitted textiles in correlation with their architecture which allows theoretical underpinnings on their design for specific performance objectives.

Acknowledgements

The authors acknowledge the financial support received by the National Science Foundation (CMMI #1537720). They also thank Professor Vadim Shapiro from the University of Wisconsin-Madison for useful discussions related to the research presented in this article.

References

ABAQUS, 2013. version 6.13, 2013. User's Manual. . Dassault Systems, Pawtucket, RI.

Abel, J., Luntz, J., Brei, D., 2013. Hierarchical architecture of active knits. Smart Materials and Structures 22, 125001.

Araujo, M., Fangueiro, R., Hong, H., 2003. Modelling and Simulation of the Mechanical Behaviour of Weft Knitted Fabric. AUTEX Journal 4.

Ashby, M., 2013. Designing architectured materials. Scripta Materialia 68, 4-7.

Au, K.-F., 2011. Advances in Knitting Technology. Woodhead Publishing

Cambridge, UK.

Barauskas, R., Abraitienė, A., 2007. Computational analysis of impact of a bullet against the multilayer fabrics in LS-DYNA. International Journal of Impact Engineering 34, 1286-1305.

Barthelat, F., 2015. Architectured materials in engineering and biology: fabrication, structure, mechanics and performance. International Materials Reviews 60, 413-430.

Bouaziz, O., Bréchet, Y., Embury, J.D., 2008. Heterogeneous and Architectured Materials: A Possible Strategy for Design of Structural Materials. Advanced Engineering Materials 10, 24-36.

Brown, L.P., Zeng, X., Long, A., Jones, A., 2013. Recent Developments in the Realistic Geometric Modelling of Textile Structures using TexGen, Proceedings of the 1st International Conference on Digital Technologies for the Textile Industries, Manchester, UK.

Carvelli, V., Corazza, C., Poggi, C., 2008. Mechanical modelling of monofilament technical textiles. Computational Materials Science 42, 679-691.

Catmull, E., Rom, R., 1974. A class of local interpolating splines, In Computer Aided Geometric Design. Eds. Academic Press, New York, New York.

Chapman, R.A., 2013. Smart textiles for protection. Woodhead Publishing, Cambridge, MA.

Choi, K.F., Lo, T.Y., 2003. An Energy Model of Plain Knitted Fabric. Textile Research Journal 73, 739-748.

Coenen, E., Kouznetsova, V., Geers, M., 2010. Computational homogenization for heterogeneous thin sheets. International Journal for Numerical Methods in Engineering 83, 1180-1205.

Cook, J.G., 1984. Handbook of Textile Fibers. Woodhead Publishing, Cambridge, England.

Demiroz, A., Dias, T., 2000. A Study of the Graphical Representation of Plain-knitted Structures Part II: Experimental Studies and Computer Generation of Plain-knitted Structures. Journal of the Textile Institute 91, 481-492.

Duan, Y., Keefe, M., Bogetti, T., Cheeseman, B., 2005. Modeling the role of friction during ballistic impact of a high-strength plain-weave fabric. Composite Structures 68, 331-337.

Duhovic, M., Bhattacharyya, D., 2006. Simulating the deformation mechanisms of knitted fabric composites. Composites Part A: Applied Science and Manufacturing 37, 1897-1915.

Farin, G., 2001. Curves and Surfaces for CAGD: A Practical Guide, 5th ed. Morgan Kaufmann.

Fillep, S., Mergheim, J., Steinmann, P., 2013. Computational modelling and homogenization of technical textiles. Engineering Structures 50, 68-73.

Fillep, S., Mergheim, J., Steinmann, P., 2015. Computational homogenization of rope-like technical textiles. Computational Mechanics 55, 577-590.

Gasser, A., Boisse, P., Hanklar, S., 2000. Mechanical behaviour of dry fabric reinforcements. 3D simulations versus biaxial tests. Computational materials science 17, 7-20.

Geers, M., Coenen, E., Kouznetsova, V., 2007. Multi-scale computational homogenization of structured thin sheets. Modelling and Simulation in Materials Science and Engineering 15, S393.

Gopalsamy, C., Park, S., Rajamanickam, R., Jayaraman, S., 1999. The Wearable Motherboard The first generation of adaptive and responsive textile structures for medical applications. Virtual Reality 4.

Green, S.D., Matveev, M.Y., Long, A.C., Ivanov, D., Hallett, S.R., 2014. Mechanical modelling of 3D woven composites considering realistic unit cell geometry. Composite Structures 118, 284-293.

Hearle, J.W.S., Shannanon, W.J., 1978. An Energy Method for Calculations in Fabric Mechanics - Part 1: Principles of the Method. Journal of the Textile Institute 69.

Hurd, J.C.H., Doyle, P.J., 1953. FUNDAMENTAL ASPECTS OF THE DESIGN OF KNITTED FABRICS. Journal of the Textile Institute Proceedings 44, P561-P578.

Jong, S.D., Postle, R., 1977. An Energy Analysis of the Mechanics of Weft-Knitted Fabrics by Means of Optimal Control Theory: Part III: The 1 x 1 Rib Knitted Structure. Journal of the Textile Institute 36.

Kaldor, J.M., 2010. Simulating Yarn-Based Cloth, Doctoral Dissertation, Department of Computer Science. Cornell University, Ithaca, New York.

Kaldor, J.M., James, S.L., Marschner, S., 2008. Simulating Knitted Cloth at the Yarn Level, ACM SIGGRAPH 2008. Association for Computer Machinery.

Karimian, M., Hasania, H., Ajeli, S., 2014. Numerical modeling of bagging behavior of plain weft knitted fabric using finite element method. Indian Journal of Fibre & Textile Research 39, 204-208.

Kiekens, P., 2012. Intelligent Textiles and Clothing for Ballistic and NBC Protection: Technology at the Cutting Edge. Springer, New York, New York.

Kothari, V., 2011. Knitted-Loop-Structure-and-Notations, Knitting Views.

Kurbak, A., Alpyildiz, T., 2009. Geometrical Models for Balanced Rib Knitted Fabrics Part II: Applications of 1 × 1 Rib Model to Presser-Foot Knitted 1 × 1 Rib, Interlock and Half Milano Rib. Textile Research Journal 79, 495-505.

Kurbak, A., Ekman, O., 2006. Basic Studies for Modeling Complex Weft Knitted Fabric. Textile Research Journal 78, 198-208.

Kurbak, A., Kayacan, O., 2008. Basic Studies for Modeling Complex Weft Knitted Fabric Structures Part V: Geometrical Modeling of Tuck Stitches. Textile Research Journal 78, 577-582.

Kurbak, A., Soydan, A.S., 2009. Geometrical models for balanced rib knitted fabrics. Part III: 2 2, 3 3, 4 4, and 5 5 rib fabrics. Textile Research Journal 79, 618-625.

Kyosev, Y., Angelova, Y., Kovar, R., 2005. 3D Modeling of Plain Weft Knitted Structures of Compressible Yarn. RJTA 9.

Leaf, G.A.V., Glaskin, A., 1955. The Geometry of a Plain Knitted Loop. Journal of the Textile Institute Transactions 46.

Lin, H., Clifford, M.J., Long, A.C., Sherburn, M., 2009. Finite element modelling of fabric shear. Modelling and Simulation in Materials Science and Engineering 17, 015008.

Lin, H., Sherburn, M., Crookston, J., Long, A.C., Clifford, M.J., Jones, I.A., 2008. Finite element modelling of fabric compression. Modelling and Simulation in Materials Science and Engineering 16, 035010.

Lin, H., Zeng, X., Sherburn, M., Long, A.C., Clifford, M.J., 2012. Automated geometric modelling of textile structures. Textile Research Journal 82, 1689-1702.

Lorussi, F., Galatolo, S., Bartalesi, R., De Rossi, D., 2013. Modeling and Characterization of Extensible Wearable Textile-Based Electrogonimeters. IEEE Sensors Journal 13.

Marculescu, D., Marculescu, R., Zamora, N., Stanley-Marbell, P., Khosla, P., Jayaraman, S., Martin, T., 2003. Electronic Textiles_A Platform for Pervasive Computing. Proceedings of the IEEE 91.

Maruccio, C., De Lorenzis, L., Persano, L., Pisignano, D., 2014. Computational homogenization of fibrous piezoelectric materials. arXiv preprint arXiv:1405.3302.

Miao, Y., Zhou, E., Wang, Y., Cheeseman, B.A., 2008. Mechanics of textile composites: Micro-geometry. Composites Science and Technology 68, 1671-1678.

Munden, D.L., 1959. The Geometry and Dimensional Properties of Plain-Knit Fabrics. Journal of the Textile Institute Transactions 50, 448-471.

Munden, D.L., 1960. DIMENSIONAL STABILITY OF PLAIN-KNIT FABRICS. Journal of the Textile Institute Proceedings 51, P200-P209.

Nadler, B., Papadopoulos, P., Steigmann, D.J., 2006. Multiscale constitutive modeling and numerical simulation of fabric material. International Journal of Solids and Structures 43, 206-221.

Park, S., Jayaraman, S., 2003. Smart Textiles: Wearable Electronic Systems.

Peirce, F.T., 1947. Geometrical Principles Applicable to the Design of Functional Fabrics. Textile Research Journal 17, 123-147.

Post, E.R., Orth, M., 2000. E-broidery: Design and fabrication of textile-based computing. IBM Systems Journal 39.

Rahali, Y., Goda, I., Ganghoffer, J.F., 2016. Numerical identification of classical and nonclassical moduli of 3D woven textiles and analysis of scale effects. Composite Structures 135, 122-139.

Renkens, W., Kyosev, Y., 2010. Geometry modelling of warp knitted fabrics with 3D form. Textile Research Journal 81, 437-443.

Sabantina, L., Kinzel, F., Ehrmann, A., Finsterbusch, K., 2015. Combining 3D printed forms with textile structures - mechanical and geometrical properties of multi-material systems, 2015 Global Conference on Polymer and Composite Materials (PCM2015), 16-18 May 2015. IOP Publishing, UK, p. 012005 (012005 pp.).

Schwartz, P., 2008. Structure and Mechanics of Textile Fibre Assemblies. Woodhead Publishing.

Semnani, D., Latifi, M., Hamzeh, S., Jeddi, A.A.A., 2003. A New Aspect of Geometrical and Physical Principles Applicable to the Estimation of Textile Structures: An Ideal Model for the Plain-knitted Loop. Journal of the Textile Institute 94, 202-211.

Sherburn, M., 2007. Geometric and Mechanical Modelling of Textiles, Doctoral Dissertation, Textile Composites. University of Nottingham, Nottingham, UK.

Spencer, D.J., 2001. Knitting Technology - A Comprehensive Handbook and Practical guide. Woodhead Publishing Series in Textiles.

Struszczyk, M.H., 2014. Design Aspects of Fibrous Implantable Medical Devices, International Congress on Healthcare and Textiles, Izmir, Turkey.

Sun, B., Hu, D., Gu, B., 2009. Transverse impact damage and energy absorption of 3-D multi-structured knitted composite. Composites Part B: Engineering 40, 572-583.

Sun, B., Pan, H., Gu, B., 2014. Tensile impact damage behaviors of co-woven-knitted composite materials with a simplified microstructure model. Textile Research Journal 84, 1742-1760.

Tran, P., Ngo, T., Yang, E.C., Mendis, P., Humphries, W., 2014. Effects of architecture on ballistic resistance of textile fabrics: numerical study. International Journal of Damage Mechanics 23, 359-376.

Vassiliadis, S.G., Kallivretaki, A.E., Provatidis, C.G., 2007. Mechanical simulation of the plain weft knitted fabrics. International Journal of Clothing Science and Technology 19, 109-130.

Wang, R., 2012. Advances in textile engineering.

Yeoman, M.S., Reddy, D., Bowles, H.C., Bezuidenhout, D., Zilla, P., Franz, T., 2010. A constitutive model for the warp-weft coupled non-linear behavior of knitted biomedical textiles. Biomaterials 31, 8484-8493.

Yuksel, C., Kaldor, J.M., James, D.L., Marschner, S., 2012. Stitch meshes for modeling knitted clothing with yarn-level detail. ACM Transactions on Graphics 31, 1-12.

Zeng, X., Brown, L.P., Endruweit, A., Matveev, M., Long, A.C., 2014. Geometrical modelling of 3D woven reinforcements for polymer composites: Prediction of fabric permeability and composite mechanical properties. Composites Part A: Applied Science and Manufacturing 56, 150-160.

Zhang, Y., Li, C., Xu, J., 2005. A micro-mechanical model of knitted fabric and its application to the analysis of buckling under tension in wale direction: buckling analysis. Acta Mechanica Sinica 21, 176-180.

Zhang, Y.T., Liu, C.Y., Du, R.X., 2007. Buckling analysis of plain knitted fabric sheets under simple shear in an arbitrary direction. International Journal of Solids and Structures 44, 7049-7060.